Systematic Projected Shell Model Study of Even-Even Dysprosium Isotopes

H. Aghahasani, S. Mohammadi*, Z. Sajjadi

Department of Physics, Payame Noor University, P.O. BOX 19395-3697, Tehran, Iran

ARTICLE INFO

ABSTRACT

Back-bending phenomenon is one of the important phenomena usually seen at high spin states of even - even heavy nuclei. As a result, any changes in the behavior of nuclear rotation, such as increase in moment of inertia versus rotational frequency can be shown in the usual back-bending plots which have been studied in many papers before. In this paper we show for the first time that these changes can be seen in the ratio of electromagnetic reduced transition probabilities B (E2) and B (M1) in even - even $^{152-164}$Dy isotopes using the Projected Shell Model (PSM) theory. The electric quadrupole transition probability B (E2) and the magnetic dipole transition probability B (M1) moments are sensitive to nuclear shape deformation and nuclear charge distribution, respectively. Our findings confirm the well-known back-bending previously seen and are in good agreement with experimental results. While intrinsic quadrupole moments are constant for each Dy isotope, the new findings show that spectroscopic quadrupole moments are increasing with spin.

INTRODUCTION

Electromagnetic study of nuclear structure is one of the important tools in high spin gamma-ray spectroscopy. The evolution of Yrast structure at high spins of neutron rich rare earth nuclei around the double mid shell have a lot of motivation to study these nuclei in recent years [1-3]. The gamma rays de-exciting the high spin states in rare earth nuclei were the subject of many studies in experimental and theoretical nuclear physics for several years. There are different models for describing the nuclear structure, where the Nilsson model that considered the deformed shape of nuclei was presented in 1955 [2]. This model accurately expresses the splitting of energy-levels due to rotational motion of deformed (non-Spherical) nucleus. In 1995, the PSM model was formulated as a shell model projected on the nuclear symmetry axis by Hara and Sun [3] which is a sum of Nilsson model and BCS theory, considering the pairing effect between nucleons. In the last two decades, this model has been used to explain a lot of high spin phenomena for heavy nuclei in rare earth nuclei. Double mid-shell nuclei with shell gaps between 50 to 82 for protons and 82 to 126 for neutrons in the lanthanide series have the largest number of valence particles, and studies show that the quadrupole deformations are high in these nuclei. There are comprehensive high spin study of nuclei in literatures [4-11]. One of the tools to study shape changes in lanthanide nuclei is back bending. This effect is related to sudden increase in moment of inertia due to breaking of pairing in nucleons at high spins. Another way to study the phenomenon of back bending is to use the ratio of reduced electromagnetic transition probabilities B (M1) and B (E2) between levels and its relation to isotopic change of shape. Even-even Dysprosium isotopes with Z=66 and N=86 to 98 are good candidates in the middle of lanthanide series to study these phenomena. Although high spin phenomena in Dy isotopes have been studied well in the past [9,10], in the present work, systematic study of shape changes in even-even $^{152-164}$Dy isotopes have been studied within PSM model using the ratio of electromagnetic transition probabilities B (M1) and B (E2) and the intrinsic and spectroscopic quadruple moments of these isotopes for the first time.

THEORY

The Spherical Shell Model (SSM) describes a nucleus as a system of independent fermions. In this

*Corresponding author.
E-mail address: smohammadi1958@gmail.com

model, each nucleon is assumed to move in an average field produced by the rest of nucleons [1]. As we go away from the shell closure, it was found that nuclei are deformed. To explain these deformed nuclei, the Nilsson model (deformed shell model) was introduced [2]. This is typically the first model used when examining data from deformed nuclei and calculating the total energy of a nucleus as a function of deformation by summation of all populated single-particle energies.

Projected Shell Model (PSM) is another deformed version of spherical shell model approach where the potential is defined in the intrinsic frame of reference that breaks the rotational symmetry spontaneously. The main advantage of the PSM approach is that it is plausible to perform a systematic analysis of high-spin band structures in a reasonable time frame with minimal computational effort.

In PSM approach the deformed basis are constructed by solving the deformed Nilsson potential with optimum quadrupole deformation parameters. The Nilsson basis states are then transformed to the quasiparticle space using the simple Bardeen-Cooper-Schrieffer (BCS) theory [12] for treating the pairing interaction to get the deformed quasiparticle basis. As a result of Nilsson + BCS calculations, a set of qp states based on a vacuum qp state |0> in the intrinsic frame was constructed. The total Hamiltonian of the PSM assumes the form in Eq. (1) [3].

$$\hat{H} = \hat{H}_0 + \frac{1}{2}\chi\sum_\mu \hat{Q}_\mu^+\hat{Q}_\mu - G_M\hat{P}^+\hat{P} - G_Q\sum_\mu \hat{P}_\mu^+\hat{P}_\mu \quad (1)$$

Here $\hat{H}_0$ is the harmonic oscillator single-particle Hamiltonian with the proper spin-orbit force. The second, third and fourth terms form the non-spherical Hamiltonian represent different kinds of characteristic correlations among active nucleus and consists of interaction terms quadrupole-quadrupole force related to deformation, monopole pairing and quadrupole pairing forces, respectively. The coefficients χ, G_M and G_Q are called the strengths of QQ + MP + QP interactions. The strength χ can be calculated self-consistently by using the quadrupole deformation parameter ε_2. All deformation parameters are chosen from Möller et al. (2016) [13].

In the rare earth region, the strength of the quadrupole pairing strengths G_Q is assumed to be proportional to G_M, $G_Q = \gamma G_M$, and the proportional constant γ is fixed as 0.16 [14]. After fixing the Hamiltonian, it is diagonalized within the shell model space spanned by a selected set of multi-quasiparticle states |Φ_k> for even-even nuclei. In this paper, the list of quasiparticle states for even-even Dysprosium isotopes which consist of (0, 2 and 4) quasiparticles for an appropriate angular momentum I are given by:

$$\{|\Phi_k >\} = \{|0>, a_{\upsilon_1}^+ a_{\upsilon_2}^+|0>, a_{\pi_1}^+ a_{\pi_2}^+|0> , a_{\upsilon_1}^+ a_{\upsilon_2}^+ a_{\pi_1}^+ a_{\pi_2}^+|0>\} \quad (2)$$

where |0> is the vacuum state and a^+ are the quasi particle (qp) creation operators and the indexυ (π) stands for neutrons (protons). More details of the PSM theory are given in Hara and Y. Sun (1995) [3].

MATERIALS AND METHODS

Electromagnetic reduced transition probabilities

The evolution of the ground-state nuclear moments such as electric quadruple moment and magnetic dipole moment provide an indication of changes in the nuclear structure, especially of shell closures. While the first one is sensitive to nuclear shape changes, the second one is a sensitive probe to the nuclear charge distribution.

Not only are the ground-state properties useful indicators for the evolution of nuclear structure, excited nuclear states can also be used to reveal the underlying shell structure. Reduced transition probabilities of the transitions between the excited states and ground state are one of the most common measures for quadrupole collectivity and shape changes in nuclei.

The reduced electric Quadrupole B (E2) and magnetic dipole B (M1) transition probabilities from an initial state I_i to a final state I_f, can be expressed as the following in Eqs. (3,4) [15,16]:

$$B(E2; I_i \rightarrow I_f) = \frac{e^2}{(2I_i+1)}|\langle I_f M_f|\hat{Q}_2|I_i M_i\rangle|^2 \quad (3)$$

$$B(M1; I_i \rightarrow I_f) = \frac{\mu_N^2}{(2I_i+1)}|\langle I_f M_f|\hat{M}_1|I_i M_i\rangle|^2 \quad (4)$$

$\hat{Q}_2$ and $\hat{M}_1$ are electric quadrupole and magnetic dipole operators respectively. Finally, by considering the partial mean life time τ_p in each transition, we obtained the reduced transition probabilities B (E2) and B (M1) as follow in Eqs. (5,6) [17-19]:

$$B(E2) = \frac{816}{E_\gamma^5 \tau_p} e^2 fm^4 MeV^5 \text{ ps (Picosecond)} \quad (5)$$

$$B(M1) = \frac{56.8}{E_\gamma^3 \tau_p} \mu_N^2 MeV^3 \text{ fs (Femtosecond)} \quad (6)$$

In the above formulas, E_γ is transition gamma energy, μ_N nuclear magneton. Calculating their ratio and omitting the mean life time τ_p for every level in Eq. (7).

$$\frac{B(M1)}{B(E2)} \cong 7 \times 10^{-5} E_\gamma^2 \frac{\mu_N^2}{e^2 \text{fm}^4} \frac{1}{\text{MeV}^2} \tag{7}$$

Which shows that their ratio is approximately proportional to E_γ^2.

Electric quadrupole moments

Another important quantity to describe quadrupole deformed nuclei is quadrupole moments. We have intrinsic quadrupole moment (Q_0) and spectroscopic quadrupole moments (Q_S). Intrinsic quadrupole moments are defined in the intrinsic body-fixed frame of the nucleus and are related to quadrupole deformation parameter ε_2 in Eq. (8) [20]:

$$Q_0 = \frac{3}{\sqrt{5\pi}} Z R_{av}^2 \varepsilon_2 (1 + 0.16\varepsilon_2) \tag{8}$$

to second order in ε_2 (ε_2 was used instead of β. $\varepsilon_2 \approx 0.95\,\beta$) .

In the above relation, Z is atomic number and $R_{av}^2 = (\frac{3}{5})R_0^2 A^{2/3}$ where $R_0 = 1.2\,fm$. The spectroscopic quadrupole moments or observed quadrupole moments are defined in the laboratory frame and are related to the intrinsic quadrupole moments by the following relation in Eq. (9) [20]:

$$Q_S = Q_0 \left[\frac{3K^2 - I(I+1)}{(I+1)(2I+3)}\right] \tag{9}$$

Where I is spin and K is its projection along symmetry axis. The parameter K has K=0 and K=2 values only. The K=0 means that the deformation is aligned along the symmetry axis and therefore preserves axial symmetry. The K=2 mode represents a dynamic time dependent excursion from axial symmetry. The dependence of Q_S on K and I means that the shape of a rotating nucleus in intrinsic and laboratory frames is different. The time averaged shape of rotation of a prolate deformed nucleus ($\varepsilon_2 > 0$) about an axis perpendicular to the symmetry axis looks like a disc, or an oblate deformed nucleus ($\varepsilon_2 < 0$). In the PSM model, we choose K=0, so $Q_S \propto -Q_0$ always.

RESULTS AND DISCUSSION

The PSM configuration space generally includes 3 major harmonic shells for protons and neutrons [3]. The calculations are done by considering 3 major shells N = 3, 4, 5 (N = 4, 5, 6) with an intruder orbital $h_{11/2}$ and shell N = 5 ($i_{13/2}$ and N = 6) for protons (neutrons). Nilsson parameters ε_2 (Quadrupole deformation) and ε_4 (Hexadecupole deformation) are chosen from Möller et al. (2016) [13] and are listed in Table 1. Also, the first excited energy (E_γ) of the first yrast level 2+ calculated by this model together with the experimental data are included in this table. As it can be seen from Fig. 1, by increasing neutron number N there is a decrease in 2+ first yrast energy, while the Quadrupole deformation increase.

Table 1. Quadrupole deformation parameter ε_2 and intrinsic neutron and proton quadrupole moments used in the present calculation. The first theoretical and experimental rast 2+ energies are also included.

Isotope (Z=66)	$\varepsilon2$	$(E\gamma)_{th}$ MeV	$(E\gamma)_{ex}$ MeV	Q_0 (protons)-barn	Q_0 (neutrons)-barn
152Dy	0.140	0.881	0.614	16.74	17.17
154Dy	0.192	0.281	0.334	22.56	23.83
156Dy	0.217	0.175	0.138	24.62	30.17
158Dy	0.242	0.120	0.099	26.24	36.51
160Dy	0.250	0.096	0.087	26.71	39.49
162Dy	0.258	0.084	0.081	27.12	42.21
164Dy	0.267	0.071	0.073	27.50	44.63
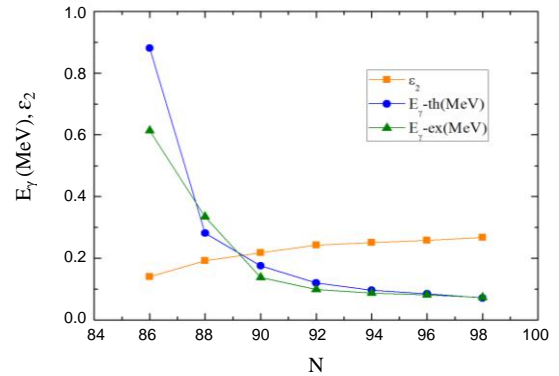
Fig. 1. First excited energy (Eγ) of the first yrast level 2+ and Quadrupole deformation ε_2 versus neutron number N for $^{152-162}$Dy isotopes.

As the electric Quadrupole (E2) and the magnetic dipole (M1) moments are sensitive to nuclear shape deformation and nuclear charge distribution, respectively, any changes in the behavior of nucleus due to rotation, such as increase in moment of inertia, can change the transition probability ratio according to Eq. (7). Figures 2 (a-f) shows back bending plots for Dy isotopes. This phenomenon occurs because the rotational energy of the nucleus exceeds the energy needed to break a pair of coupled nucleons.
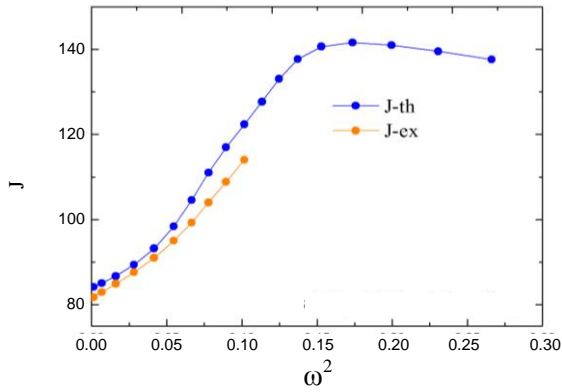
(a). Dy-164 back bending.
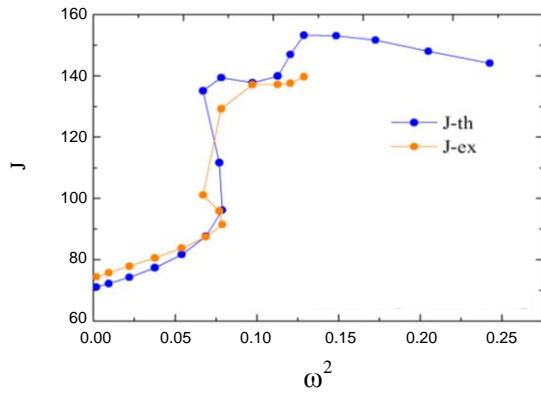
(b). 162-Dy back bending.
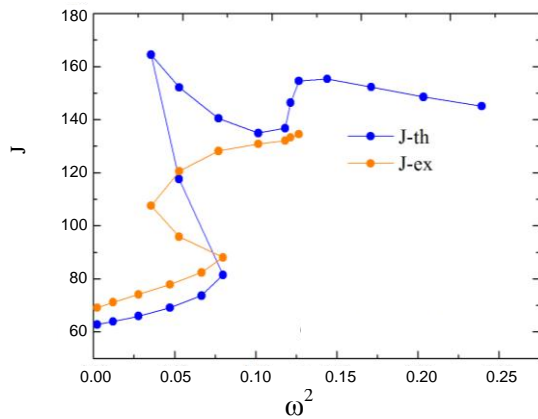
(c). 160-Dy back bending.
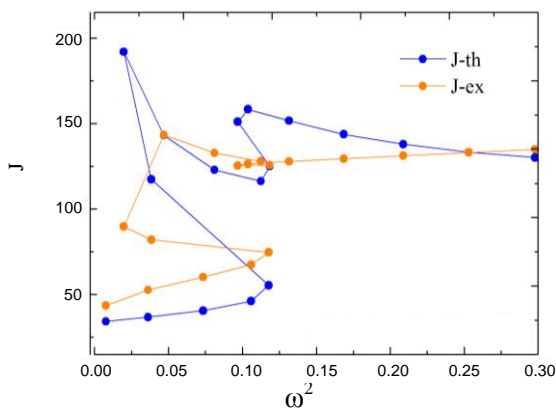
(d). 156-Dy back bending.
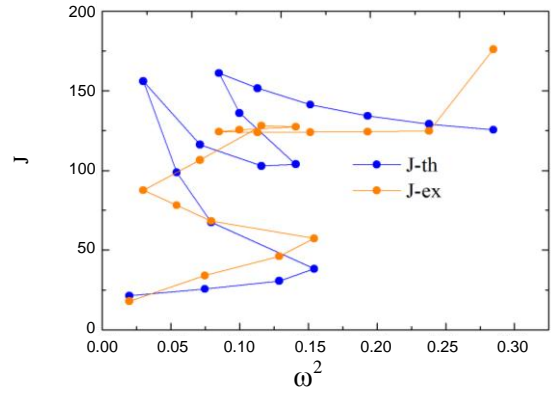
(e). 154-Dy back bending.
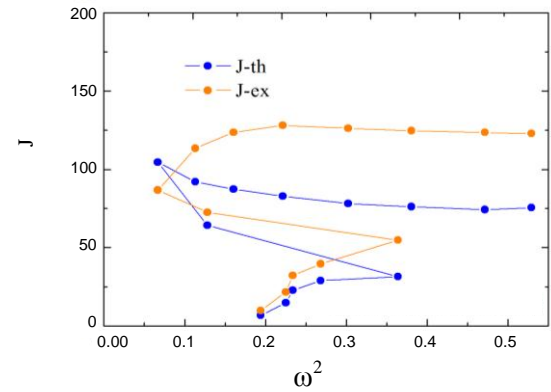
(f). 152-Dy back bending.

Fig. 2 (a-f). Back bending plots for even-even Dy isotopes. Moments of inertia (J) versus squared angular frequency (ω^2). The data for [158]Dy were not included in this figure due to some irregularities in data.

The unpaired nucleons then go into different orbits and increase the nuclear moment of inertia at some spins which cause reduction in nuclear rotation, so it looks like a back bending in the diagrams. Our calculations are a little different from calculations of Velazquez, et al. [9] due to different input data to PSM code. Also, more experimental data are available in this paper for comparison. The moment of inertia J is defined as $J = \frac{4I-2}{E(I)-E(I-2)}$ ($\frac{\hbar^2}{MeV}$) and rotation speed ω as $\omega = \frac{E(I)-E(I-2)}{2}$ [21]. All experimental data for excitation states are taken from Ref [22]. The data for [158]Dy were not included in Fig. 2 due to some irregularities in data.

Figure 3 shows electromagnetic reduced transition probabilities ratio B (M1) /B (E2) versus spin I for Dy isotopes calculated from formula 7. Again, all experimental data are taken from Radware (2021) [22]. For [152]Dy, the electromagnetic transition ratio B(M1)/B(E2) increases gradually with increasing spin up to I = 10 ħ and suddenly drops up to spin 14 ħ. This means that at first the behavior of the nucleus is mostly magnetic dipole transitions with a gradual increase in the contribution of the electric quadrupole transitions, as spin increases. This is the range of spin which back bending phenomenon occurs in [152]Dy, as shown in Fig. 2.
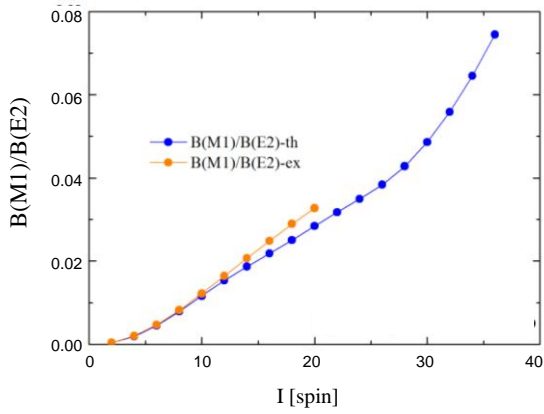
(a). 164-Dy transition ratio.
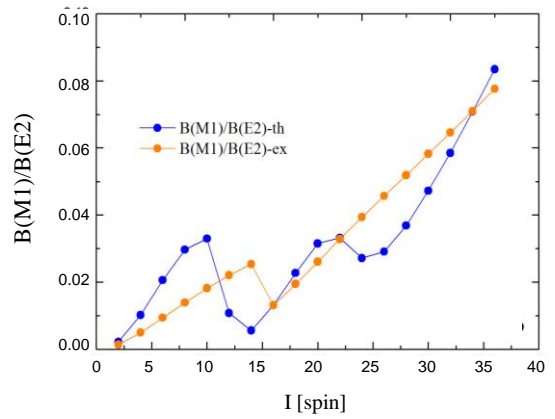
(b). 162-Dy transition ratio.
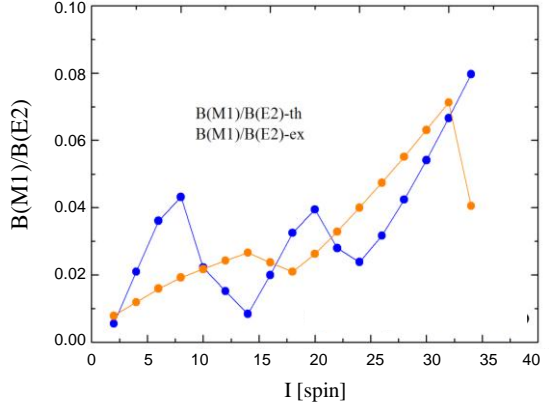
(c). 160-Dy transition ratio.

(d). 158-Dy transition ratio.

(e). 156-Dy transition ratio.

(f). 154-Dy transition ratio.
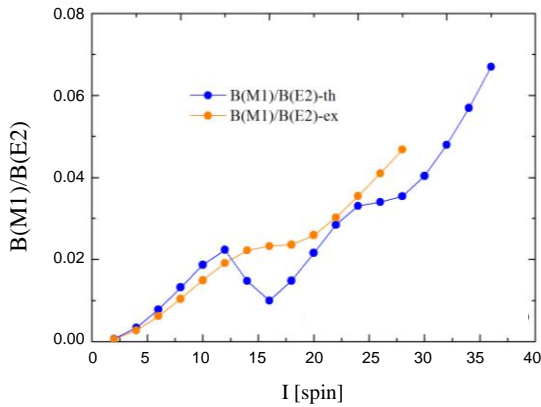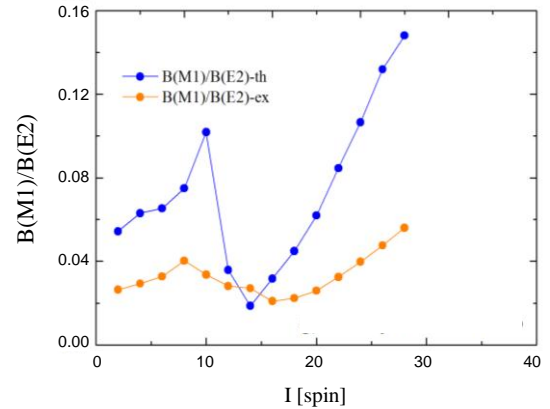
(g). 152-Dy transition ratio.

Fig. 3 (a-g). Electromagnetic reduced transition probabilities ratio B (M1) /B (E2) versus spin I for Dy isotopes.
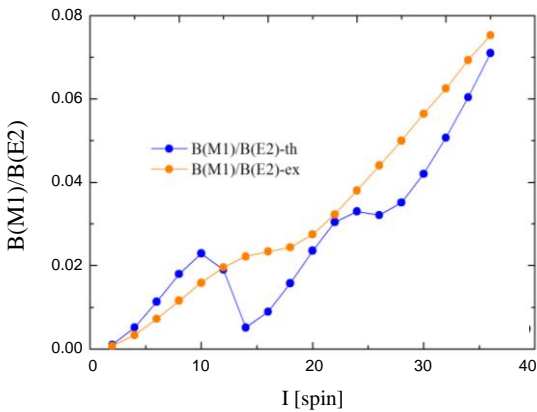
In other words, as nuclear rotational motion increases due to alignment of $h_{9/2}$ 2qp-neutrons in I = 10 ℏ, the rotating motion suddenly decrease with increasing in moment of inertia, and this happens with reductions in the dipole magnetic properties. As is well known, the breaking of nucleon pairs causes back bending. For [154]Dy, the same rising and dropping occurs for alignment of $h_{9/2}$ 2qp neutron + $h_{11/2}$ 2qp proton at spins I = 8 ℏ and 20 ℏ, which is related to another back bending in [154]Dy. The same trend happens for [156]Dy at spins I = 10 ℏ and 22 ℏ, for [158]Dy at spins I = 10 ℏ and 24 ℏ, for [160]Dy at spins I = 12 ℏ and 24 ℏ, and for [162]Dy at spins I = 14 ℏ and 26 ℏ.

Band-crossings occur in all Dy isotopes irrespective to whether they show a back-bending or not (up-bending). The first band that crosses the g-band is referred to as the "s-band". The question is why the lighter isotopes show better back-bending and the heavier ones up-bending. The answer is that a back-bending (up-bending) occurs if the crossing angle between two bands is large (small). The reason is as follows. If the crossing angle is large, the g- and s-band do not admix each other except at the nearest vicinity of the crossing point because they are mostly well separated energetically from each other. Therefore, the transition from the g-band to s-band takes place suddenly. This is the back-bending. On the other hand, if the crossing angle is small, the g- and s-bands will stay close to each other for a relatively large spin interval so that they can easily admix with each other all the way and, therefore, the transition between them occurs rather gradually. This is the up-bending, which can be seen in Fig. 2. This is also the reason for discrepancies in B (M1) /B (E2) ratio in Figs. 3(a-g). Table 2 shows all theoretical calculations and experimental datavvvv used for ^{162}Dy. All items in the table has been defined in the text. The same tables have been prepared for other isotopes as well, however, to save space they are not shown here. Figures 2 and 3 show all the calculations and comparison with experimental results.

The last two columns in Table 1 show intrinsic neutron and proton quadrupole moments Q_0 for Dy isotopes. As it can be seen, this quantity for neutrons has a higher value relative to protons at ground state which is related to placement of neutrons at higher orbitals. Both quantities are constant in the intrinsic body-fixed frame of the nucleus. Figures 4 and 5 show the spectroscopic or observed quadrupole moments Q_S which are defined in the laboratory frame and are calculated from equation 9. These quantities are increasing with spin for both neutrons and protons which shows quadrupole shape changes and is more prominent for neutrons than protons for heavier isotopes which is again related to placement of neutrons at higher orbitals. Due to unavailability of experimental data for the spectroscopic quadrupole moments of even-even Dy isotopes, no comparison was done.
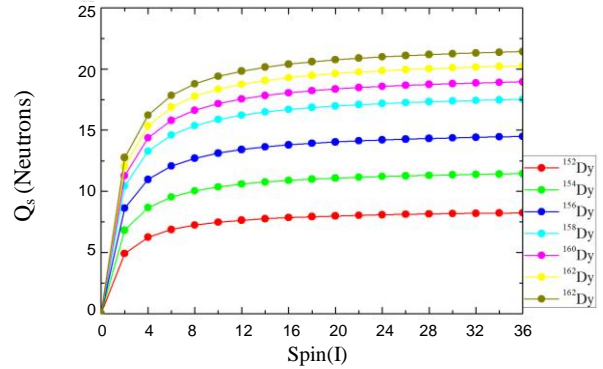
Fig. 4. Neutron spectroscopic quadrupole or observed quadrupole moments (Q_S) versus spin I for Dy isotopes.
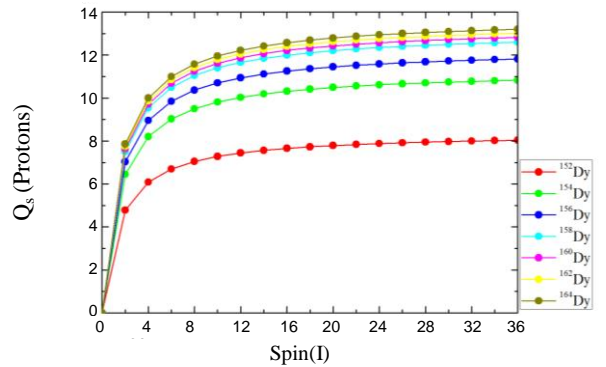
Fig. 5. Proton spectroscopic quadrupole or observed quadrupole moments (Q_S) versus spin I for Dy isotopes.

Table 2: Theoretical and experimental Data for ^{162}Dy Isotope.

I(Spin)	ΔE (th.) MeV	ω^2 (th.)	J (th.) (Inertia)	$\left[\frac{B(M1)}{B(E2)}\right]_{th.} = 0.07(\Delta E)^2_{th.}$	ΔE (ex.) MeV	J (ex.) $= \frac{4I-2}{\Delta E(ex.)}$ (Inertia)	$\left[\frac{B(M1)}{B(E2)}\right]_{ex.} = 0.07(\Delta E)^2_{ex.}$
2	0.0845	0.0018	71.0377	0.0004	0.0807	74.3494	0.0004
4	0.1940	0.0094	72.1646	0.0026	0.1849	75.7166	0.0023
6	0.2964	0.0220	74.2210	0.0061	0.2827	77.8210	0.0055
8	0.3881	0.0376	77.3080	0.0105	0.3725	80.5369	0.0097
10	0.4654	0.0541	81.6588	0.0151	0.4536	83.7742	0.0144
12	0.5247	0.0688	87.6661	0.0192	0.5262	87.4192	0.0193
14	0.5618	0.0789	96.1205	0.0220	0.5906	91.4324	0.0244
16	0.5552	0.0771	111.678	0.0215	0.6470	95.8268	0.0293
18	0.5181	0.0671	135.101	0.0187	0.6924	101.0976	0.0335
20	0.5596	0.0783	139.391	0.0219	0.6037	129.2032	0.0255
22	0.6243	0.0974	137.758	0.0272	0.6272	137.1173	0.0275
24	0.6718	0.1128	139.920	0.0315	0.6854	137.1461	0.0328
26	0.6943	0.1205	146.917	0.0337	0.7415	137.5590	0.0384
28	0.7178	0.1288	153.256	0.0360	0.7873	139.71802	0.0433
30	0.7711	0.1486	153.035	0.0416	-	-	-
32	0.8309	0.1726	151.638	0.0483	-	-	-
34	0.9054	0.2049	147.997	0.0573	-	-	-
36	0.9851	0.2426	144.145	0.0679	-	-	-

CONCLUSION

Shape changes for even - even $^{152\text{-}164}$Dy isotopes using the ratio of electromagnetic reduced transition probabilities B (E2) and B (M1) and spectroscopic quadrupole moments for high-spin states up to spin 36 ℏ have been studied by using the PSM model and compared with available experimental data. These findings confirm the well-known back-bending seen by drawing moments of inertia versus squared angular frequency where lighter isotopes show better back-bending and the heavier ones up-bending which is related to crossing angle between ground and "S' bands. In fact, the back-bending phenomenon which is related to the breaking of nucleon pairs and their alignments with nuclear core rotation has been observed also as changes in the ratio of electromagnetic reduced transition probabilities.

In this work, as the neutron number increases for each Dysprosium isotope, these electromagnetic ratio changes were observed to happen at higher spins which is related to more shape deformation. The spectroscopic or observed quadrupole moments Q_S which are defined in the laboratory frame, are also increasing with spin for both neutrons and protons which are more prominent for neutrons than protons for heavier isotopes. This behavior is related to higher intruder orbital $i_{13/2}$ for neutrons than the intruder orbital $h_{11/2}$ for protons where more rotation coupling with core is expected for protons.

ACKNOWLEDGEMENT

AUTHOR CONTRIBUTION

Hosniye Aghahasani is the main contributor to this paper. All other authors read and approved the final version of the paper.

REFERENCES

1. B. M. Nyako, J. Timar, M. Csatlos *et al.,* Phys. Rev. **104** (2021) 054305.

2. S. M. Lenzi, A. Poves and A. O. Macchiavelli, Phys. Rev. **104** (2021) L031306.

3. K. Hara and Y. Sun, Intern. J. Mod. Phys. **04** (1995) 637.

4. V. Kumar, A. Kumar and and P. C. Srivastava, Nucl. Phys. **1017** (2021) 122344.

5. S. Aydin, M Ionescu-Bujor, N. Marginean *et al.,* Phys. Rev. **104** (2021) 054309.

6. A. Barzakh, A. N. Andreyev, C. Raison *et al.,* Phys. Rev. Lett. **127** (2021) 192501.

7. C. Babcock, H. Heylen, M. L. Bissel *et al.*, Phys. Lett. **760** (2022) 387.

8. V. Rani, S. Singh, M. Rajput *et al.,* Eur. Phys. J. **57** (2021) 274.

9. V. Velaquez, J. G. Hirsch, Y. Sun *et al.,* Nucl. Phys. **653** (1999) 355.

10. Z. Wen-Hua and G. Jian-Zhong, Chin. Phys. Lett. **27** (2010) 012101.

11. M. Shahriarie, S. Mohammadi and Z. Firouzi, J. Korean Phys. Soc. **76** (2020) 8.

12. H-T. Kim, Sci. Rep. **11** (2021) 1.

13. P. Möller, A. J. Sierk, T. Ichikawa *et al.,* Atomic Data and Nuclear Data Tables, **109-110** (2016) 1.

14. J. A. Sheikh, Y. Sun and P. M. Walker, Phys. Rev. **57** (1998) R26.

15. K. Rajesh, Mod. Phys. Lett. **33** (2018) 1850188.

16. S. Shen, F. Wang, J. Shen *et al.,* Phys. Open **9** (2021) 100091.

17. V. Rani, P. Verma, S. Singh *et al.,* Chin. Phys. **44** (2020) 094107.

18. T. Islam, R. Amin, R. Alam *et al,* J. Nucl. Sci. Technol. **10** (2020) 129.

19. B. K. Usta and S. Eser, Acta Phys. Pol. **137** (2020) S1-S42.

20. H. Zanganeh, A. Kardan and M. H. H. Yazdi, J. Nucl. Sci. Technol. **41** (2020) 32.

21. H. Ryde, Eur. Phys. J. **46** (2021) 1.

22. Anonymous, Oak Ridge National Laboratory. https://radware.phy.ornl.gov/. Retrieved in August (2021)